



## Recent surface cooling in the Yellow and East China Seas and the associated North Pacific climate regime shift

Yong Sun Kim<sup>a</sup>, Chan Joo Jang<sup>a,b,\*</sup>, Sang-Wook Yeh<sup>c</sup>

<sup>a</sup> Ocean Circulation and Climate Research Center, Korea Institute of Ocean Science and Technology, Busan, Republic of Korea

<sup>b</sup> Department of Integrated Ocean Sciences, University of Science and Technology, Daejeon, Republic of Korea

<sup>c</sup> Department of Marine Sciences and Convergent Technology, Hanyang University, ERICA, Ansan, Republic of Korea

### ARTICLE INFO

#### Keywords:

Sea surface temperature (SST)  
Yellow and East China Sea (YECS)  
Pacific Decadal Oscillation (PDO)  
Siberian High  
Regime shift  
Kuroshio Current

### ABSTRACT

The Yellow and East China Seas (YECS) are widely believed to have experienced robust, basin-scale warming over the last few decades. However, the warming reached a peak in the late 1990s, followed by a significant cooling trend. In this study, we investigated the characteristics of this low-frequency sea surface temperature (SST) variance and its dynamic relationship with large-scale climate variability through cyclostationary orthogonal function analysis for the 1982–2014 period. Both regressed surface winds on the primary mode of the YECS SST and trends in air-sea heat fluxes demonstrate that the intensification of the northerly winds in winter contribute largely to the recent cooling trend by increasing heat loss to the atmosphere. As a localized oceanic response to these winds, the upwind flow seems to bring warm waters and partially counteracts the basin-scale cooling, thus contributing to a weakening of the cooling trend along the central trough of the Yellow Sea. In the context of the large-scale climate variabilities, a strong relationship between the YECS SST variability and Pacific Decadal Oscillation (PDO) became weak considerably during the recent cooling period after the late 1990s as the PDO signals appeared to be confined within the eastern basin of the North Pacific in association with the regime shift. In addition to this decoupling of the YECS SST from the PDO, the intensifying Siberian High pressure system likely caused the enhanced northerly winds, leading to the recent cooling trend. These findings highlight relative roles of the PDO and the Siberian High in shaping the YECS SST variance through the changes in the large-scale atmospheric circulation and attendant oceanic advection.

### 1. Introduction

The Yellow and East China Seas (hereafter YECS) consist of a shallow, semi-closed basin located in the northwest Pacific Ocean (Fig. 1). Its southern boundary is delimited by the sharp continental slope along the Okinawa Trough, which separates the YECS from the main axis of the Kuroshio Current. Including the central trough, the majority of the YECS is shallower than 100 m with a mean depth of 75 m. Hence, nutrients supplied from the bottom via intense turbulent and tidal mixing, as well as from the rivers surrounding the YECS, form one of the broadest and most productive marine ecosystems in the world (Belkin, 2009), having socioeconomic implications of climate change for the people living around the YECS (e.g., Xie et al., 2002). Therefore, it is essential to understand the climatic evolution of the YECS SST and the underlying climate dynamics.

Due to these implications, many studies have studied extensively the long-term variability of the SST in the YECS (Xie et al., 2002; Belkin, 2009; Yeh and Kim, 2010; Zhang et al., 2010; Kim et al., 2013; Oey

et al., 2013; Wang et al., 2013; Bao and Ren, 2014; Park et al., 2015; Wu et al., 2016, 2017; Pei et al., 2017). A broadly accepted conclusion from these studies might be encapsulated in that the YECS has experienced a robust, persistent SST increase in the last few decades at the rates of 2–4 times faster than the globally averaged trend, i.e., 0.13 °C per decade (Trenberth et al., 2007). This warming trend has been explained by various dynamics including anthropogenic effects from the industrialized countries around the YECS (Belkin, 2009; Bao and Ren, 2014), discharged riverine water effects (Belkin, 2009; Park et al., 2011), anomalous heat supplies associated with oceanic advection (Zhang et al., 2010; Wang et al., 2013), and decreased air-sea turbulent heat loss to the atmosphere as a result of weakened winds particularly for the winter monsoon (Yeh and Kim, 2010; Oey et al., 2013; Park et al., 2015).

Recent studies, however, have started to report a slowdown of the warming trends (Bao and Ren, 2014), and even cooling trends along coastlines (Liao et al., 2015). Fig. 2a shows the monthly time series of the SST anomalies averaged over the YECS (29°N–41°N, 117°E–129°E)

\* Correspondence to: Korea Institute of Ocean Science and Technology, 385 Haeyang-ro, Yeongdo-gu, Busan 49111, Republic of Korea.  
E-mail address: [cjang@kiost.ac.kr](mailto:cjang@kiost.ac.kr) (C.J. Jang).

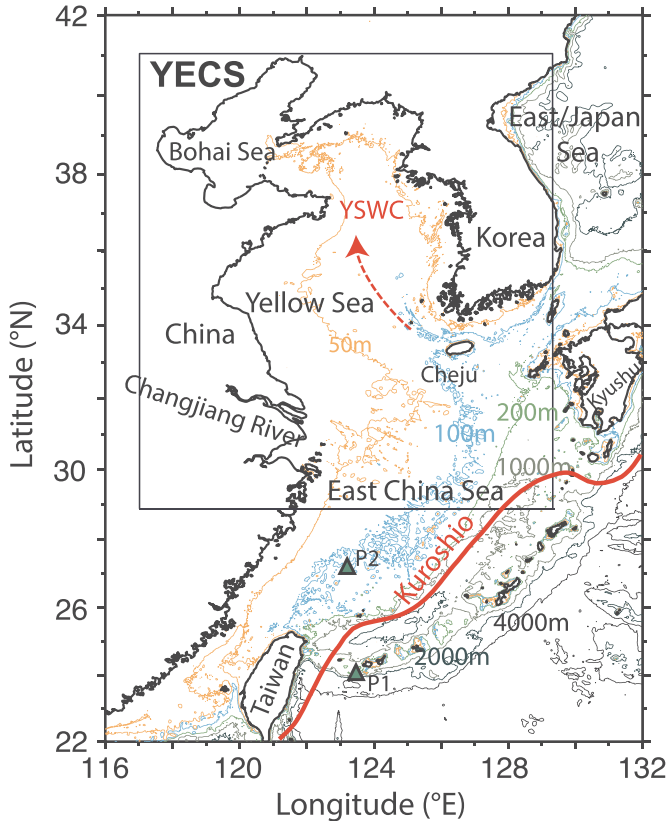


**Fig. 1.** (a) Topography around the Yellow and East China Seas; the thin contours are bathymetry with 50, 100, 200, 1000, 2000, and 4000-m labeled. The red arrow shows the Yellow Sea Warm Current (YSWC). The thick red line is the 1.15-m sea surface height contour denoting the mean path of the Kuroshio. The two triangles indicate the geographical locations of P1 ( $24^{\circ}\text{N}$ ,  $123.5^{\circ}\text{E}$ ) and P2 ( $27.25^{\circ}\text{N}$ ,  $123.25^{\circ}\text{E}$ ) to calculate the SSH difference for the Kuroshio volume transport through the East Taiwan channel. (For interpretation of the references to color in this article, the reader is referred to the web version of this article.)

for the period 1982–2014. The most striking evolution pattern is that a robust warming trend at a rate of  $+0.40^{\circ}\text{C}$  per decade reached a peak in the late 1990s, and then it turned downward at a rate of  $-0.36^{\circ}\text{C}$  per decade. The positive and then negative trends are estimated throughout the YECS for the periods 1982–1997 (Fig. 2b) and 1998–2014 (Fig. 2c) respectively, indicating that the trend reversal is a basin-scale and low-frequency variance. As a result, this trend reversal yields a much weaker positive trend than that in previous studies over a period longer than the last three decades. A potential mechanism leading to this low-frequency variance has not been discussed much in the literature so far. Liao et al. (2015) noted, for instance, this recent cooling trend along the Chinese and Japanese coastlines, presumably as a result of the intrinsic nature of the climate in association with the recent intensification of the East Asian winter monsoon, but without any proof being put forward for the causal relation between the cooling and atmospheric circulation.

In the meantime, it is well documented that the variability of the YECS SST is connected to the Pacific in the context of natural variabilities including El Niño–Southern Oscillation (ENSO; e.g., Park and Oh, 2000; Wang et al., 2000; Wu et al., 2016, 2017), the North Pacific Oscillation (NPO; Yeh and Kim, 2010), and the Pacific Decadal Oscillation (PDO; Zhang et al., 2010; Kim et al., 2013; Liao et al., 2015). Interestingly, recent studies have indicated that the North Pacific experienced an abrupt, systematic change associated with the unusual thermal changes in the tropical Pacific, that is, the 1997–1998 El Niño (Yeh et al., 2009; Di Lorenzo et al., 2010; Yeo et al., 2012; Xiang et al., 2013; Liao et al., 2015; Jo et al., 2015). The reported changes can be most likely summarized in the term of “regime shift”, which can be characterized by 1) the central Pacific warming-type El Niño having

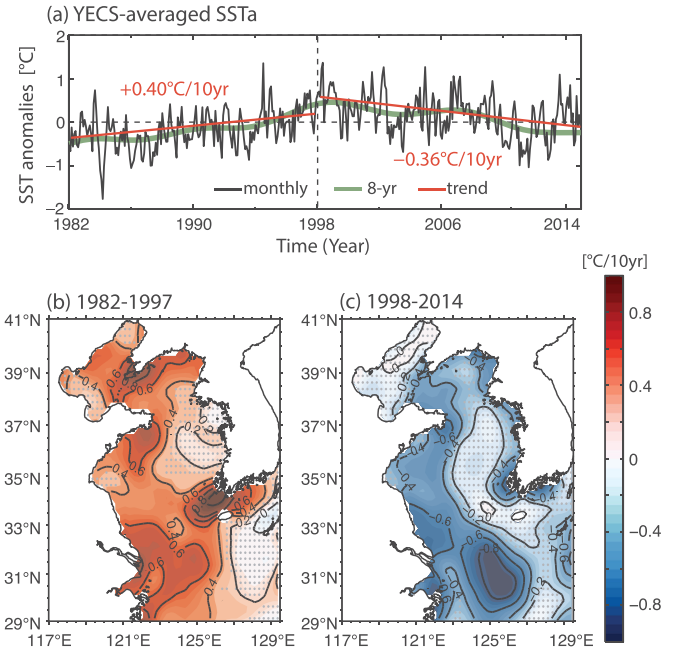


**Fig. 2.** (a) Time series of the monthly sea surface temperature (SST) anomaly averaged in the Yellow and East China Seas (black); the thick green and red lines indicate the 8-year low pass filtered SST anomaly and the trends for the periods 1982–1997 and 1998–2014, respectively. The spatial distributions of the linear SST trends are illustrated for the periods (b) 1982–1997 and (c) 1998–2014, respectively. The gray dots show that the trends are insignificant trends at the 95% confidence level.

occurred more frequently than the typical eastern Pacific warming type El Niño (Yeh et al., 2009; Yeo and Kim, 2014); 2) the North Pacific Gyre Oscillation (NPGO), defined as the 2nd sea surface height mode in the eastern North Pacific (Di Lorenzo et al., 2008, 2010), becoming dominant and its amplitude outpacing that of the 1st SST mode, i.e., PDO (Bond et al., 2003; Di Lorenzo et al., 2010); 3) the low-frequency PDO index entering a negative phase from a positive one (Peterson and Schwing, 2003; Overland et al., 2008; Deser et al., 2010; Jo et al., 2015; Newman et al., 2016).

From the fact that the YECS is geographically located in the northwest Pacific, as well as from the timing of the trend reversal in the YECS coinciding with the regime shift, it can be inferred that the regime shift in the North Pacific is somehow related to the decadal SST trend reversal in the YECS. The goal of this study is to investigate this hypothesis. For this purpose, we analyzed the satellite-based optimum interpolation SST version 2 (OISSTv2) dataset by applying the cyclostationary empirical orthogonal function (CSEOF). In Section 2, the details of the methods are presented along with the brief descriptions of data sets and climate indices used in the study. The leading SST modes for the 1982–2014 period are identified via the CSEOF analysis in Section 3. Then, in Section 4, we examine the relationship of the leading mode and its corresponding atmospheric circulation and oceanic components, which have been suggested as key dynamics in shaping the YECS SST variability. The oceanic and atmospheric changes associated with the regime shift in the North Pacific before and after the regime shift are investigated in Section 5. We suggest a candidate mechanism for the recent cooling trend in Section 6. A summary and concluding remarks follow in the final section.

## 2. Data and methodology

### 2.1. SST dataset

The primary SST dataset analyzed in this study is the daily Advanced Very High Resolution Radiometer (AVHRR)-based OISSTv2 (Reynolds et al., 2007; obtained from <http://www.esrl.noaa.gov/psd/>

[data/gridded/data.noaa.oisst.v2.html](#)). A monthly mean SST dataset for the period 1982–2014 (i.e., 33 years) was used in this study. Considering that the study area of the YECS covers only 12.5° longitudes by 12° latitudes (i.e., 117–129.5°E, 29–41°N), we believe that the OISSTv2 is the most suitable SST dataset for this study due to its fine spatial resolution (i.e., 1/4° × 1/4°) without degrading or a systematic bias for more than three decades (e.g., Reynolds and Chelton, 2010). The advantage of this dataset is apparent when compared with other gridded datasets such as the Hadley Center Ice and Sea Surface Temperature (HadISST; 1° horizontal resolution), the Extended Reconstructed Sea Surface Temperature version 4 (ERSSTv4; 2° resolution), and the Operational Sea Surface Temperature and Sea Ice Analysis (OSTIA, 1/20° resolution), which spans only the period since 2007.

## 2.2. Ancillary observations and climate indices

To investigate the underlying dynamics for the observed SST variability, we explored a range of ancillary datasets describing the atmospheric and oceanic status. For the atmospheric circulation, we used the monthly time series of surface winds at 10 m and the sea level pressure (SLP) from the European Centre for Medium-range Weather Forecasts (ECMWF) Interim (available online at <http://www.ecmwf.int>) for the period 1982–2014. The satellite-based Cross-Calibrated Multi-Platform (CCMP) (Atlas et al., 2009) wind from 1988 to 2014 and the Global Data Assimilation System (GODAS; Behringer, 2007) net heat flux from 1982 to 2014 were also used to compute the linear trends and other statistics. A positive sign for the heat flux indicates a downward flux from the air into the ocean. This study compared the temporal evolution of the YECS SST with the large-scale climate indices for 1982–2014 including the PDO index (Mantua et al., 1997; available online at <http://research.jisao.washington.edu/pdo/PDO.latest>), the NPGO (Di Lorenzo et al., 2008; <http://www.o3d.org/npgc/npgc.php>), the Nino 3.4 SST for ENSO ([https://www.esrl.noaa.gov/psd/geos\\_wgsp/Timeseries/Data/nino34.long.data](https://www.esrl.noaa.gov/psd/geos_wgsp/Timeseries/Data/nino34.long.data)), and the Arctic Oscillation (AO; [http://www.cpc.ncep.noaa.gov/products/precip/CWlink/daily\\_ao\\_index/monthly.ao.index.b50.current.ascii.table](http://www.cpc.ncep.noaa.gov/products/precip/CWlink/daily_ao_index/monthly.ao.index.b50.current.ascii.table)). For the oceanic status, we analyzed the volume transports of the Kuroshio (1993–2014) suggested by Yan and Sun (2015) and of the Changjiang River water Discharge (CRD; 1982–2011) provided by the Bureau of Hydrology at the Changjiang Water Resources Commission.

## 2.3. CSEOF analysis

Empirical orthogonal function (EOF) analysis is a common method, which can provide statistical insights into physical processes in an intricate climate system. This method decomposes a target variable into a number of spatial loading vectors and their corresponding temporal evolutions based on the assumption of stationarity (or time independency) in the temporal evolutions. This assumption, however, is often inappropriate since a general geophysical variable tends to have a strong annual cycle, thus likely yielding non-stationarity even after removing the long-term mean annual cycle. This non-stationarity may lead to the possibility of getting a result with an inaccurate modal decomposition (e.g., Kim, 1997; Kim et al., 2015). To deal with this problem, we adopted the CSEOF method, which achieves the stationarity further by adding a periodicity (or cyclostationary) assumption to the loading vectors (Kim et al., 2015): a target variable (i.e., SST anomalies in this study after removing a long-term mean annual cycle),  $T(x, t)$ , is decomposed into cyclostationary loading vectors (CSLVs),  $A_n(x, t)$ , and the corresponding PC time series,  $PC_n(t)$  as:

$$T(x, t) = \sum_n A_n(x, t) PC_n(t) \quad (1)$$

Here,  $n$  is a mode number;  $x$  and  $t$  denote space and time, respectively. Because of the periodicity assumption,  $A_n(x, t) = A_n(x, t+d)$ , where  $d$  is a pre-determined period. We set this period to 12 months to represent

an annual cycle. This analysis thereby allows us to investigate a seasonal cycle for an identified mode along with twelve maps of the CSLVs.

Another advantage of using the CSEOF method is the extraction of a regressed field that evolves to be more physical and statistically consistent with a specific target PC than with one from a typical regression method, which generally postulates a linear relationship between the target and the predicted variables (refer to Section 5 of Kim et al. (2015) and the references therein for more information). To estimate the regressed field for a predictor variable (surface wind anomalies in this study), the predictor variable was also decomposed into the loading vectors,  $AP_m(x, t)$ , and the PC time series,  $PCP_m(t)$ . Then, a number of the extracted  $PCP_m(t)$  are regressed onto a specific target,  $PC_n(t)$ , by finding out the regression coefficients,  $a_n^{(m)}$ , in a way that minimizes the variance of the regression error time series,  $\epsilon_n(t)$ :

$$PC_n(t) = \sum_{m=1}^M a_n^{(m)} PCP_m(t) + \epsilon_n(t), \quad n = 1, 2, \dots \quad (2)$$

The regressed spatial patterns for the predictor variable,  $AP_n(x, t)$ , are then estimated as:

$$AP_n(x, t) = \sum_{m=1}^M a_n^{(m)} AP_m(x, t) \quad (3)$$

As a result, the regressed field shares the PC of the target variable at the level of the regressed error.

## 2.4. Statistical significance test

Note that the p-value is estimated based on a student's  $t$ -test to examine the significance in various statistical analyses. Results rendering a p-value of less than 0.05, for instance, are considered statistically significant at the 95% confidence level. An autocorrelation inherent to the time-series is also considered to determine the degree of freedom and the p-value, as suggested by Bretherton et al. (1999).

## 3. Results

The monthly averaged SST anomalies in the YECS are decomposed into a number of CSLVs and their corresponding PC time series for the 33-year period, i.e., 1982–2014. Fig. 3a and b illustrate the leading PC time series and the corresponding CSLVs, respectively. Note that the PC time series has been normalized with a unit variance, and the CSLVs are plotted in units of °C. This leading mode accounts for approximately 25% of the total variance, and is clearly separated from the other minor modes based on a lead-lag correlation analysis (Yeo and Kim, 2014). It is worth noting that the explained variance reached 50% when this mode was calculated using a conventional EOF method. This EOF PC of course shows a significant correlation ( $r=0.89$ ,  $p<0.01$ ) with the PC time series from the CSEOF analysis (see Supplementary Fig. S1). Furthermore, we compared the PC time series estimated from the OISSTv2 with the SSTs from the HadISST and ECMWF Interim reanalysis datasets. The fact that the PC estimated from these two datasets matches well with the one from the OISSTv2 ( $r=0.87$  and 0.92, respectively) provides evidence for the insensitivity of the study to the SST datasets. The leading mode is also shown to be insensitive to the meridional span of the domain (not shown).

Unsurprisingly, the CSEOF PC1, as shown in Fig. 3a, represents well the characteristic evolution pattern depicted in Fig. 2a: a significant positive trend of 1.26 per decade by the late 1990s turns into a negative trend at a rate of −0.91 per decade. When compared with the EOF modes reported in previous studies, this PC1 is quite similar to the leading PC estimated with the winter mean SST for the period 1950–2008 (Yeh and Kim, 2010; see their Fig. 2b). From the two leading modes estimated from the seven-year low-pass filtered SST in China's coastal seas for the period 1900–2006 (Zhang et al., 2010), the leading mode from this study seems to correspond to their second

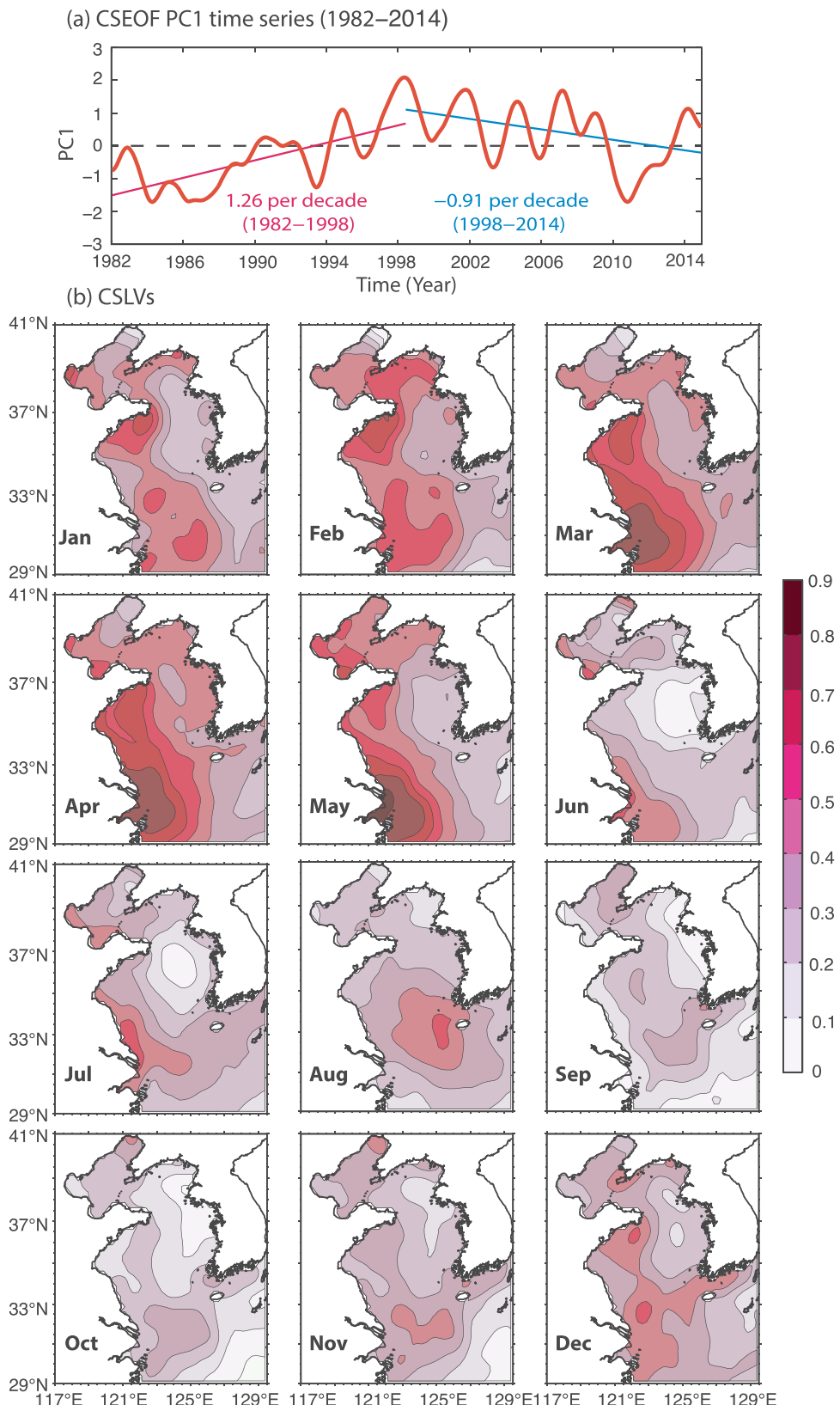


**Fig. 3.** (a) Principal component time series and the corresponding loading vectors for the first cyclostationary empirical orthogonal function (CSEOF) mode of the sea surface temperature anomalies over the Yellow and East China Seas for the period 1982–2014.

mode, which represents the PDO variability within the China's seas, rather than their first mode for global warming (see Section 5 for details).

Fig. 3b shows an enhanced variance appearing in the western basin

of the YECS; positive anomalies higher than  $0.4^{\circ}\text{C}$  extend from the mouth of the Changjiang River toward the northwest along the Chinese coast during the winter and spring months, while anomalies extend toward the East/Japan Sea during the summer and fall months. On the

other hand, a relatively weak variance is observed in the eastern basin of the Yellow Sea, where the variance for the second mode is comparable to that of the basin mode, especially during the summer months (not shown). As the second mode appears to represent interannual fluctuations linked to the ENSO teleconnection, the year-to-year SST variance is likely to predominate in the eastern basin. Fig. 3b also reveals that the variance of the CSLVs is about three times higher for the winter and spring months than for the summer and fall months, with a maximum appearing in March and April. This is further supported by the basin mode estimated from a typical EOF method: the EOF1 pattern as shown in Fig. S1a has the highest correlation with the CSLVs for April ( $r=0.85$ ) and the lowest correlation with those for June ( $r=0.33$ ). Thereby, we have focused on the winter to spring SST variability hereafter and its dynamics in the context of the large-scale atmospheric variabilities and local oceanic variabilities around the YECS.

#### 4. Dynamics

A heat budget analysis is a common tool for exploring the roles of the various dynamics in generating a temperature change inside a water column. Unfortunately, publicly available reanalysis datasets have some difficulties in simulating long-term evolution in coastal currents (Zhang et al., 2010), along with a lack of information on vertical entrainment at the base of a mixed layer. Therefore, the following section focuses on the individual roles of atmospheric and oceanic components in generating the basin mode of the YECS SST anomalies based on regression and correlation analyses.

##### 4.1. Atmospheric components: wind and heat flux

Fig. 4 displays the winter (January, February, and March) mean regressed ECMWF Interim surface wind field onto the CSEOF PC1 time series estimated from the YECS SST anomalies for the period 1982–2014. The regressed values represent changes corresponding to a positive unit standard deviation of the PC1; hence, the physical meaning of the regressed vectors is how a change in the surface wind is associated with a positive anomaly of the PC1, that is, a SST increase. Fig. 4 illustrates that the regressed winter winds can be characterized by southerly wind anomalies. The prevailing winds during the winter

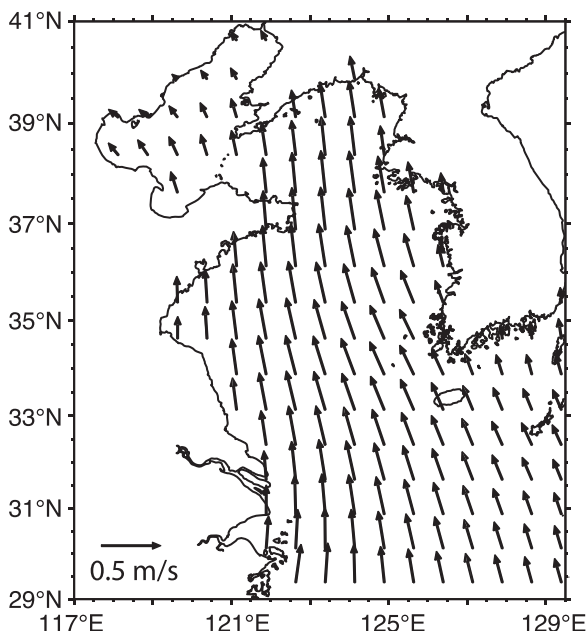


Fig. 4. The winter (January–February–March) mean regressed map of the surface wind at 10 m vectors against the first principal component for the Yellow and East China Seas SST anomalies.

monsoon are northwesterly winds, which bring cold and dry air from the continent, thereby leading to huge heat loss from the ocean to the atmosphere. As a result, the southerly wind anomalies are indicative of a weakened winter monsoon due to the decreased loss of turbulent heat to the overlying atmosphere. With regard to the decadal trend reversal of the CSEOF PC1, a similar tendency but in the opposite way occurred after 1998, that is, an intensified winter monsoon accompanied by northerly wind anomalies.

This trend reversal of the winds and the attendant change in the heat fluxes were also inferred from a linear trend analysis using the satellite-based CCMP winter winds (Fig. 5a–b) and net heat fluxes of the GODAS data, simulated with National Centers for Environmental Prediction–Department of Energy (NCEP–DOE) AMIP-II wind stress (Fig. 5c–d). The southwesterly trends (i.e., decreasing wind speed) before 1998 turned into northeasterly trends (i.e., increasing wind speed) for the period after 1998. As expected from the relationship between wind and heat flux, the winter heat fluxes appeared with a positive (negative) trend, probably leading to the basin-scale sea surface warming (cooling) anomalies for the period before (after) 1998. The winter mean trend of the net heat fluxes over the YECS amounts to  $3.9 \pm 2.3 \text{ W/m}^2$  per year and  $-2.9 \pm 2.0 \text{ W/m}^2$  per year for the periods before and after 1998, respectively. With the assumption of that the water column is fully mixed during a cold season (Chu et al., 1997), the rates of  $0.98 \pm 0.58 \text{ }^\circ\text{C}$  per decade for the period 1982–1998 and  $-0.73 \text{ }^\circ\text{C} \pm 0.5 \text{ }^\circ\text{C}$  per decade for 1998–2014 were simply inferred from a mixed layer heat balance equation (Stevenson and Niiler, 1983). These rates seem to go somewhat further than the actual trends estimated from the SST in Fig. 2a, but reasonable when considering not only the lack of heat flux for the northern part of the Yellow Sea in the GODAS data, but also oceanic advection with surface winds acting as a damping effect (refer Section 6). It is worth noting that such a distinct trend in the net heat fluxes was not estimated for the heat flux datasets from ECMWF Interim and objectively analyzed air-sea flux (OAFlux). This discrepancy is likely due to the heat fluxes calculations being associated with large uncertainties not only in atmospheric-oceanic variables including air/sea temperatures, wind speed, and humidity, but also in the parameters of the bulk formula (Weare, 1989; Pei et al., 2017). According to Na et al. (1999), these uncertainties even tend to increase during a cold season, along with the increasing role of wind speed in the calculation of turbulent heat fluxes.

While we believe that a decadal change in atmosphere causes the variation of the winter SSTs in the YECS, the opposite is also possible. Simultaneous correlations between heat flux and SST, and between heat flux and SST tendency can be useful indicators to examine the relative importance of SST forcing versus convective forcing in local air-sea interaction (Wu et al., 2006). In case of the SST forcing on the atmosphere, there will be a large negative correlation between heat flux and SST since the positive SST anomalies are able to cause increasing heat loss to the atmosphere (i.e., negative heat flux anomalies) and vice versa. On the other hand, a positive correlation between heat flux and SST tendency might be estimated when a change in the heat flux causes the SST variability. Fig. 6 shows these correlations calculated with monthly mean anomaly time series after removing the long-term mean annual cycle using the GODAS heat flux and the OISSTv2 for the 1982–2014 period. Before the calculation, the SST was interpolated to the heat flux grid; the SST tendency was calculated based on centered differencing. Apparent are weak but positive correlations for the heat flux–SST and heat flux–SST tendency throughout the study domain for the winter months. The low-pass filtering does not change the result qualitatively. These correlations seem to highlight the role of the atmospheric forcing in shaping the basin-scale SST variability over the YECS especially during the cold season (Wei et al., 2013).

##### 4.2. Oceanic components: the Kuroshio and Changjiang River

Besides atmospheric forcing, several studies have argued that even a

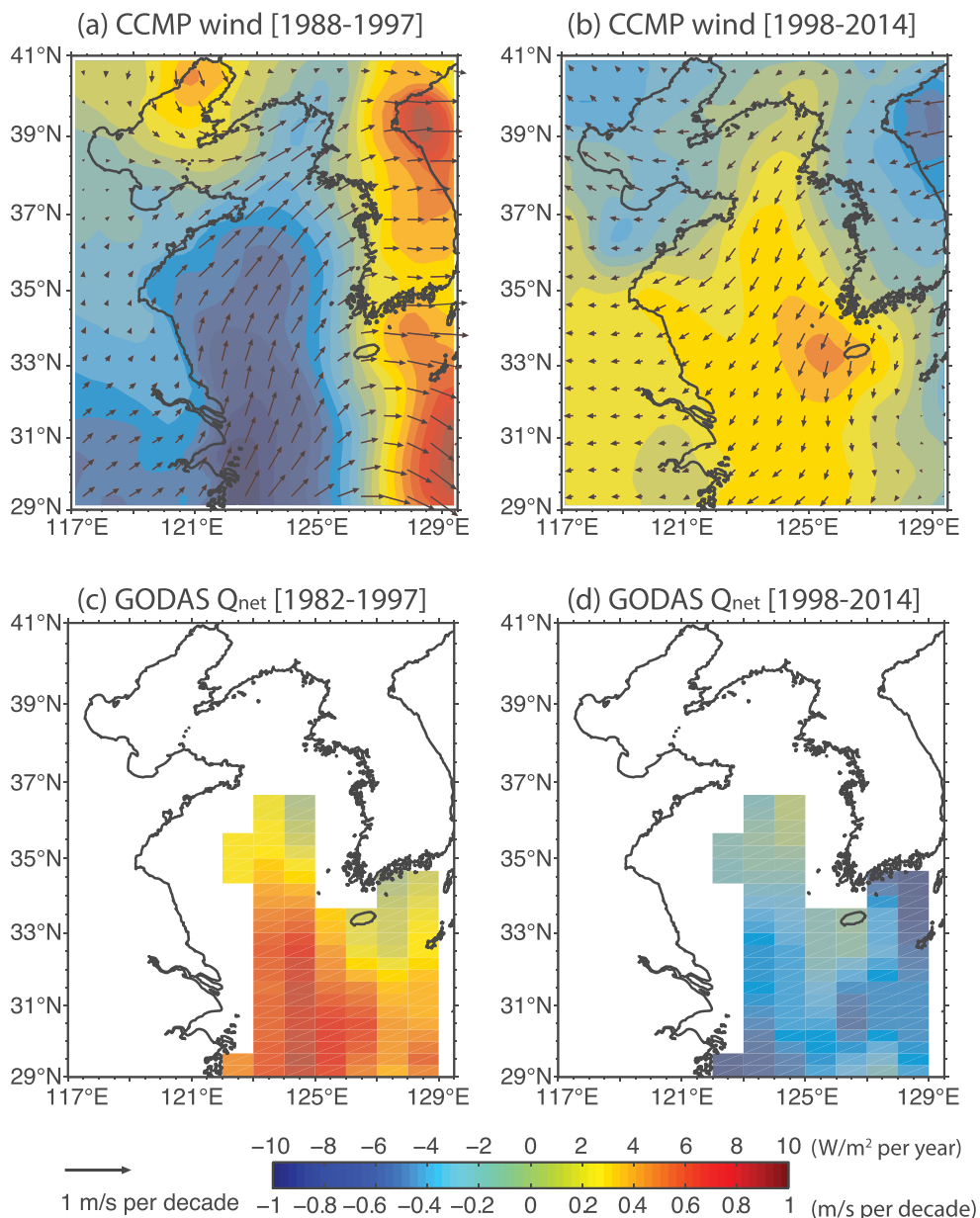


**Fig. 5.** Linear trends of winter (JFM) mean (a–b) CCMP wind speed (shading: m/s per decade) and vectors (arrows: m/s per decade) and (c–d) GODAS net heat fluxes ( $\text{W}/\text{m}^2$  per year; positive downward) for the periods before (left) and after 1998 (right).

subtle change in the Kuroshio Current might result in a considerable influence on the water properties of the YECS (Zhang et al., 2010; Park et al., 2012; Wang et al., 2013). To examine this argument, we utilized the altimetry-based Kuroshio Volume Transport (KVT) time series, defined as the sea level difference (SLD) between P1 (123.5°E, 24°N) and P2 (123.0°E, 26.5°N) in the East Taiwan Channel:  $\text{KVT} = 0.31 \times \text{SLD}_{\text{P}_1, \text{P}_2} + 6.55$  (Yan and Sun, 2015). The estimated transport was transformed into standardized time series (Fig. 7a). When we compared the KVT index with the CSEOF PC1 estimated from the YECS SST anomalies, the correlation coefficient between the two time series was not as high as 0.25 (Fig. 7b). The highest, but still insignificant correlation appeared when the KVT index preceded the PC1 by two months. This poor relationship might suggest that the role of the Kuroshio is not enough to determine the basin-scale SST variance, in consistence with previous studies (Kim et al., 2013; Wei et al., 2013; Pei et al., 2017).

Nevertheless, oceanic advection can bring a local SST change, especially during winter when the strong northerly winds are dominant. We performed a time-lagged correlation analysis to estimate the

relationship between the KVT index and late winter (February–March–April, FMA) mean SST anomalies. Unsurprisingly, significant and positive correlation coefficients appeared along the main path of the Kuroshio along the Okinawa Trough, as an instantaneous response of the SST to the Kuroshio transport (Fig. 8a). This is in line with that the Kuroshio arrives at the western edge of this study's domain in around 17 days with the assumption of a mean speed of the Kuroshio of about 1 m/s (Yan and Sun, 2015). As the lag increased, a signal of positive correlations appeared to extend northwestward toward the central trough of the Yellow Sea. The highest correlation coefficients ( $r > 0.60$ ;  $p < 0.05$ ) were estimated between the two-month preceded KVT index and the SST in the center of the Yellow Sea (Fig. 8b), and the significant correlations higher than 0.5 continued for four months (Fig. 8c). These relationships along the path of the local Kuroshio branch are consistent with the generally accepted view of that the Kuroshio feeds the Yellow Sea Warm Current (YSWC) as an upwind flow during the winter monsoon (Ichikawa and Beardsley, 2002; Isobe, 2008; Lin et al., 2011; Tak et al., 2016).

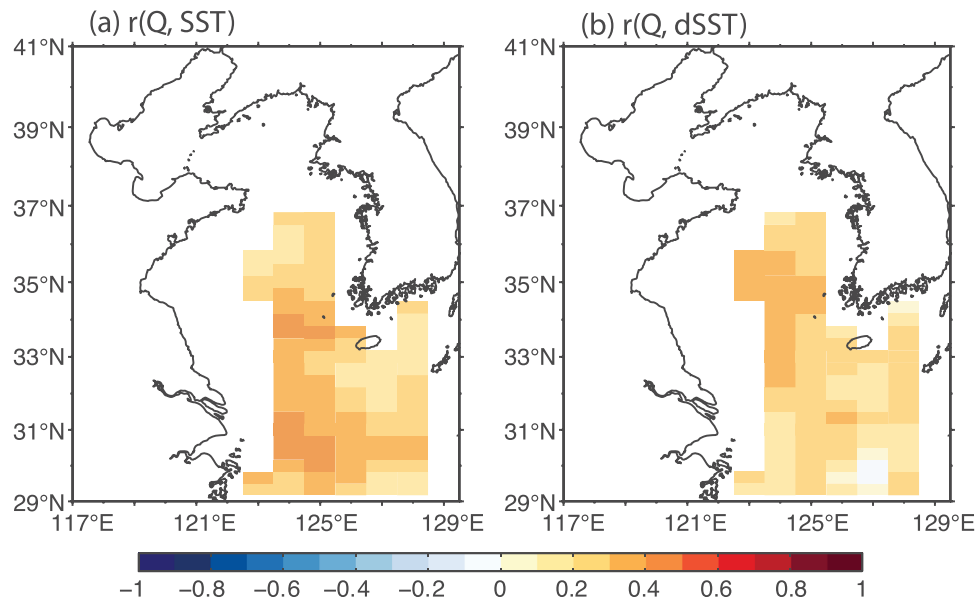


**Fig. 6.** Point-wise and simultaneous correlations (a) between net heat flux and SST and (b) between net heat flux and SST tendency derived from the GODAS heat flux and the OISSTv2 data sets for the winter months (February–April) of 1982–2014.

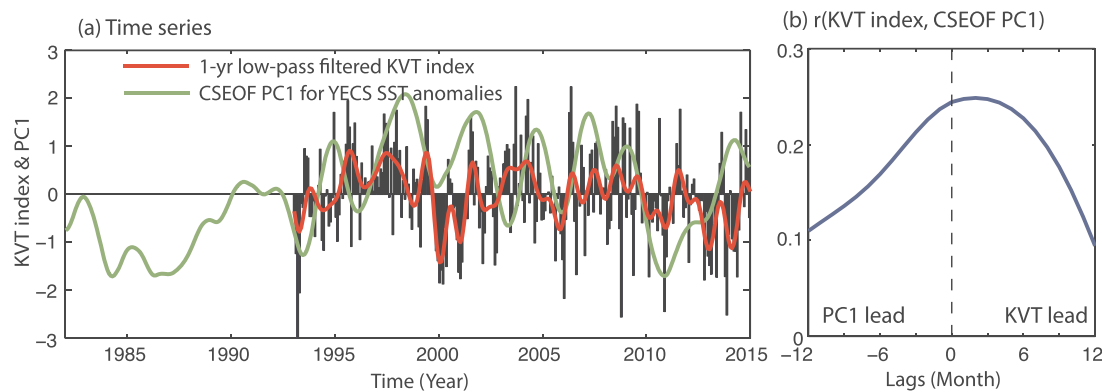


**Fig. 7.** (a) Monthly time series of the Kuroshio volume transport (KVT) index (black bars) and its 1-year low pass filtered time series (red line) along with the first principal component for the YECS SST anomalies (green line) and (b) the lead-lag correlations between the 1-year low pass filtered KVT index and the CSEOF PC1 time series.

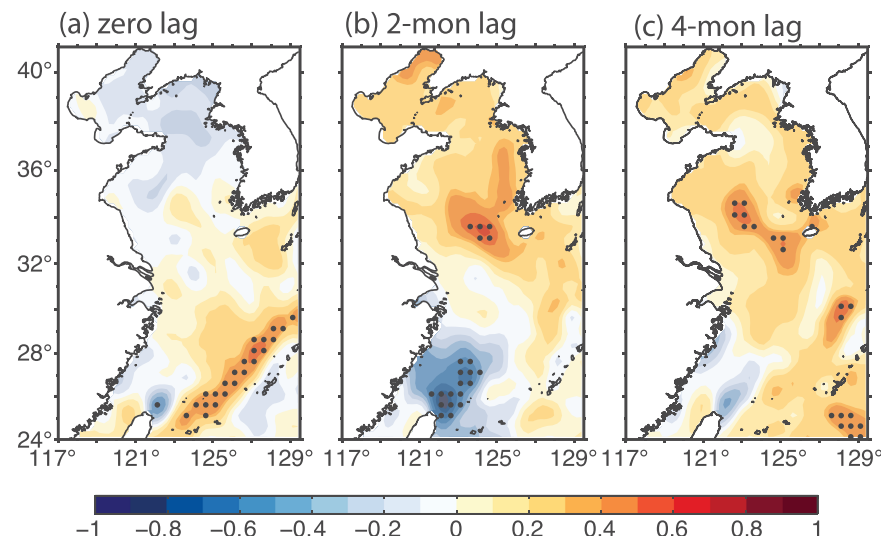


**Fig. 8.** Lagged correlations between the preceding altimetry-based Kuroshio volume transport index and the FMA mean SST anomalies (fixed) for the period 1993–2014. The dots superimposed on the correlation maps show the regions where the correlations are statistically significant at the 95% confidence level based on a student's *t*-test.

The discharged waters from the Changjiang River have a tendency to become warmer both by trapping solar radiation within a barrier layer and by reducing vertical heat diffusion and entrainment across the lower boundary of the layer (Belkin, 2009; Park et al., 2011). Hence, one might anticipate a climatic implication associated with the variance of the discharge waters. In fact, Yang et al. (2015) reported a 65% reduction in the river's discharges during a recent decade (2003–2012) compared to that of the previous decade (1993–2002) due to a decline in precipitation over the Changjiang catchment after the construction of the Three Gorges Dam. This reduction may have also resulted in the decadal SST variance. However, significant correlations could not be found between the late winter SST and the volume of the discharged waters in the region around the mouth of the river. When we performed a lead-lag correlation analysis between the CRD and the FMA SST time series for the period 1982–2011, relatively high correlations appeared not along the Chinese coast but along the Korean coast, particularly when the SST preceded the CRD by one month (not shown). This unexpected result might hint that the discharged waters do not have a considerable impact at least on the late winter SST anomalies, possibly because the volume of the discharged waters in winter is only a quarter of that of the summer maximum. There may be a common mechanism that controls both the discharged volume transport of the riverine waters and the late winter SST in the eastern basin of the Yellow Sea. Further analysis is, however, beyond the scope of this study.

## 5. The dynamic relationship between the YECS and the North Pacific

To assess the dynamic relationship between the YECS SST and the large-scale climate variability around the YECS, we calculated the correlations of the CSEOF PC1 shown in Fig. 3a with climate modes including the PDO, NPGO, AO, and Nino 3.4 indices. For this calculation, we applied a 1-year Butterworth window to these monthly time series to filter out high-frequency signals. The estimated correlation coefficients are summarized in Table 1. Among these modes, the PC1 correlated negatively with the PDO index at the 95% confidence level, but only for the period 1982–1997 (Table 1; see Fig. 9a). Consistently, the area-averaged winter net heat flux over the YECS, which was estimated using the GODAS dataset, had a significant relationship with the PDO for the 1982–1997 period ( $r = -0.61$ ), and the relationship became weak afterwards ( $r = 0.18$ ). Another demonstration of limited YECS SST and PDO coupling is provided by applying an 11-year moving window to the correlation analysis (Fig. 9b). The statistically significant correlation coefficients down to  $-0.70$  continued until 1997, while their correlations practically vanished during the period after the late 1990s. This abrupt change can be understood as that the SST variability in the YECS being closely linked to the North Pacific as a part of the PDO system as demonstrated by Zhang et al. (2010), but for a limited period before the North Pacific regime shift (Kim et al., 2013; Liao et al., 2015).

As mentioned above, one of the noticeable climate changes that occurred during the late 1990s is that the NPGO became more prevalent with a greater amplitude than a PDO signature (Bond et al., 2003; Di Lorenzo et al., 2010; Yeo et al., 2012; Jo et al., 2015). This systematic

**Table 1**

Correlation coefficients between the time series of the CSEOF PC1 estimated from the YECS SST and 1-year low pass filtered climate indices including the Pacific Decadal Oscillation (PDO), the North Pacific Gyre Oscillation (NPGO), the Arctic Oscillation (AO), and the Nino3.4 SST. The correlations marked in bold indicate that the correlation is statistically significant at the 95% confidence level.

Periods	PDO	NPGO	AO	Nino3.4
1982–2014	– 0.25	+ 0.10	+ 0.18	+ 0.15
1982–1997	<b>– 0.60</b>	– 0.32	+ 0.43	+ 0.21
1998–2014	+ 0.17	– 0.10	+ 0.27	+ 0.18

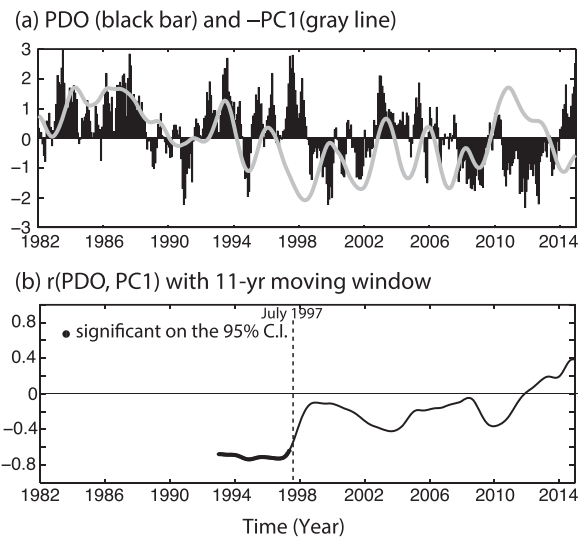


**Fig. 9.** (a) Time series of the first principal component (PC1, thick gray line) estimated from the CSEOF analysis using the YECS SST anomalies and the Pacific Decadal Oscillation (PDO) index (bars), and (b) the 11-year moving correlation coefficients between these two time series. Note that we have plotted minus PC1 in (a) to show its negative relationship with the PDO. In (b), the last year of each moving period is plotted on the x-axis.

change might have had a non-trivial impact on the YECS climate. Yeh and Kim (2010), for instance, argued that the winter SST variance in the YECS was dynamically linked to the NPO-like anticyclonic atmospheric circulation, i.e., the atmospheric expression of the NPGO (Di Lorenzo et al., 2008, 2010). Therefore, one might anticipate that the role of the PDO in relation to the YECS SST variance would have been superseded by the NPGO after the late 1990s. The CSEOF PC1 of the YECS SST and the 1-year filtered NPGO index, however, were scarcely correlated ( $r = -0.10$ ; Table 1), even for the period after the regime shift, which is indicative of the negligible influence of the NPGO (or NPO) on the YECS SST in this recent period. Low correlations have been also estimated with other climate modes including the AO and the ENSO both before and after the regime shift (see Table 1). This abrupt change in the connectivity between the YECS and the Pacific Ocean becomes more evident from the correlation maps between the CSEOF PC1 of the YECS SST and the North Pacific SST anomalies (Fig. 10). A comparison between Fig. 10a and b demonstrates that the wide, tongue-like region (i.e., the central North Pacific) with significant correlations before the late 1990s has distinctly shrunk to the seas around the YECS.

What happened during the late 1990s, when the North Pacific is believed to have entered a new climate regime? The large-scale atmospheric and oceanic features associated with the regime shift are depicted in Fig. 11. Here, the fractions of the SST and SLP, which are linearly congruent with the PDO, are provided for the periods before and after the late 1990s, respectively. The PDO index for each period was calculated as the EOF PC1 time series from the extratropical North Pacific ( $110^{\circ}$ – $260^{\circ}$ E,  $20^{\circ}$ – $65^{\circ}$ N) SST anomalies. The index is, of course, nearly identical to the Mantua PDO index. Before the regime shift, it is immediately apparent that the strong, negative SLP anomalies were widespread throughout the North Pacific (Fig. 11a). The corresponding SST field featured a broad band of negative anomalies between  $30^{\circ}$ N and  $45^{\circ}$ N. The band extended from the Northwest Pacific practically to the whole basin while being surrounded by weak, positive anomalies. These spatial distributions of the SLP and SST anomalies are the canonical atmospheric and oceanic signatures for the positive phases of the PDO (Mantua et al., 1997; Wu and Liu, 2003; Hartmann, 2015; Newman et al., 2016). After the regime shift, in contrast, the SLP anomaly diminished slightly in its strength along with its center moving southeastward to the eastern North Pacific (Fig. 11b). Concurrently, the band of negative SST anomalies was marginally noticeable, while

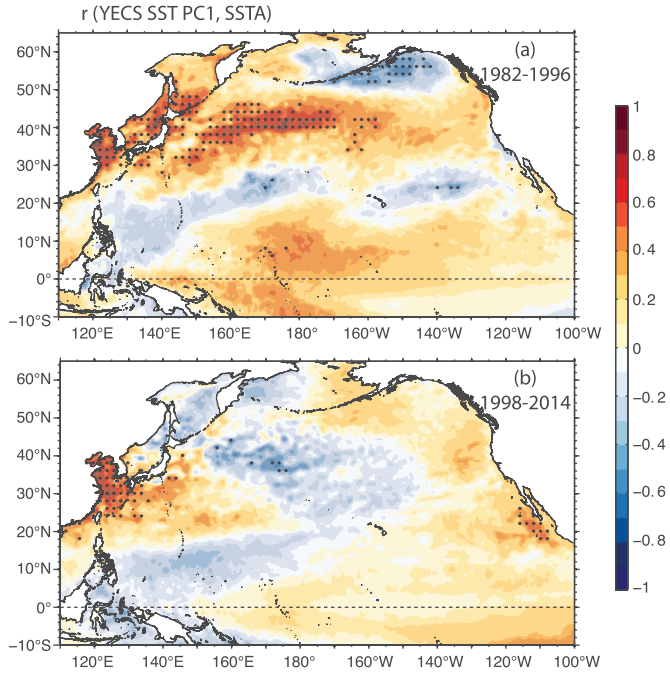


**Fig. 10.** Correlation maps between the monthly time series of the first CSEOF principal component for the YECS SST anomalies and the 1-year low pass filtered SST anomalies in the North Pacific for the periods (a) 1982–1997 and (b) 1998–2014. The dots superimposed on the correlation maps indicate that the correlations are statistically significant at the 95% confidence level based on a student's *t*-test.

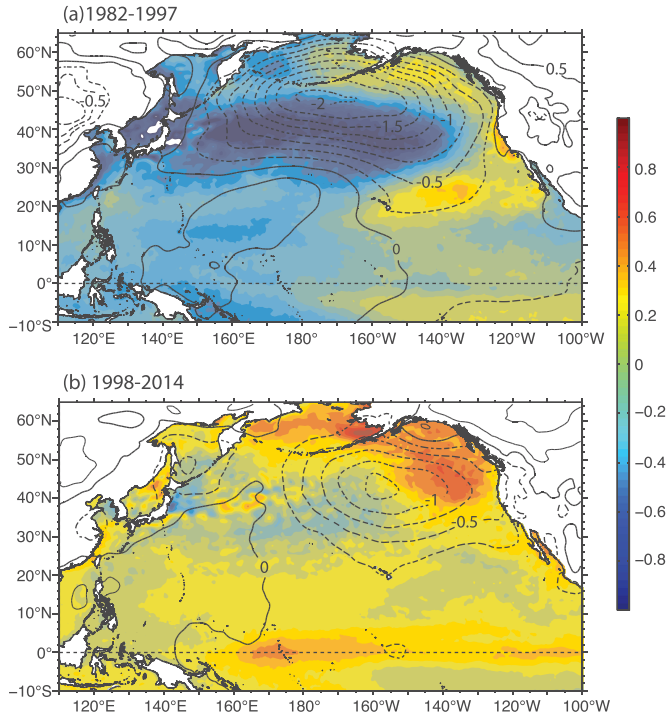


**Fig. 11.** Linearly regressed maps of the SST (unit: °C, shading) and SLP (unit: hPa, contours) onto the first EOF principal component time series estimated from the extratropical North Pacific SST anomalies for the periods (a) 1982–1997 and (b) 1998–2014. The contour interval is 0.25 hPa; the solid contours are for the positive SLP and the dashed contours for the negative SLP anomalies.

positive SST anomalies from the Bering Sea to the south of the Gulf of Alaska were recognizable by their strong amplitude along the coast of the North America. These linearly regressed SLP/SST patterns share some degree of similarity with that of the NPGO (Yeo et al., 2012; Wen

et al., 2014; Ding et al., 2015), and are consistent with many studies that have reported an increase of NPGO-related SST signals in recent decades (Bond et al., 2003; Di Lorenzo et al., 2010; Wen et al., 2014; Yeo et al., 2014). For example, Wen et al. (2014) identified that the SST pattern, which was associated with the recent PDO, displayed a NPGO-like pattern relative to the early period owing to the non-stationarity of the PDO. Figs. 10 and 11 display collectively that the oceanic/atmospheric signals associated with the PDO have been somewhat limited to the eastern basin of the North Pacific during the recent period. In other words, the PDO, although it is the basin mode in the North Pacific, had a reduced impact on the SST of the western basin after the regime shift, which contributes at least in part to the recent decoupling of the YECS from the influence of the PDO.

## 6. A possible mechanism for the recent cooling trend in the YECS

One question that needs to be answered, then, is what has been controlling the recent cooling trend in the YECS? We are focusing on the fact that the YECS are in a location that is under the influence of the Siberian High (SH), which is known to have intensified since the 1990s (Jeong et al., 2011; Li and Wang, 2013; Ding et al., 2014; Liao et al., 2015; Xie et al., 2016). Hence, the temporal variability of the SST in the YECS might have been facilitated more by the SH when the connectivity of the YECS to the North Pacific became weaker during the recent period. To examine this hypothetical relationship, we illustrated the time series of the SH index (the black bars in Fig. 12a) and the late winter (FMA) mean CSEOF PC1 for the YECS SST anomalies (the gray line in Fig. 12a). The index was calculated here as the standardized DJF mean SLP in the northwestern Mongolia region between 40°–65°N and 80°–120°E by following Jeong et al. (2011), and thus the index represents the winter mean intensity of the SH pressure system. Note that we used the FMA mean CSEOF PC1 to reflect the delayed SST response to atmospheric forcing, as well as because the strongest relationship actually appeared between the index and the two-month lagged SST anomalies.

As expected from this hypothesis, a contrasting relationship between the CSEOF PC1 and the SH index can be found before and after the late 1990s; these time series were barely correlated ( $r = -0.26$ )

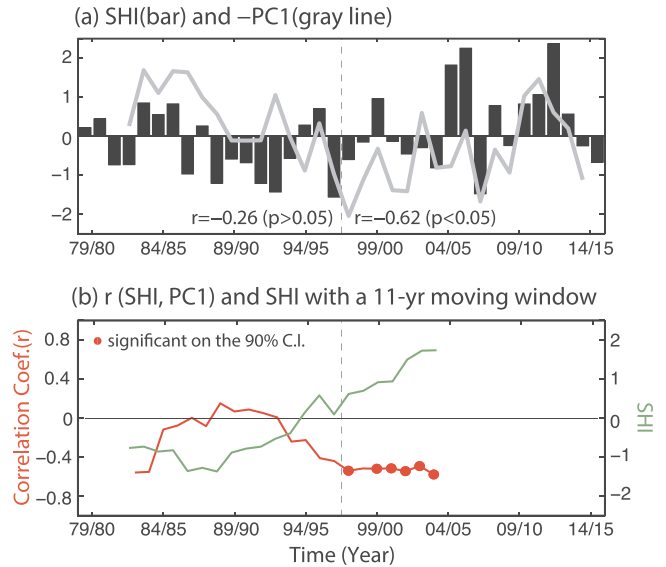


**Fig. 12.** (a) Time series of the normalized intensity of the Siberian High (bars) and the corresponding FMA mean first CSEOF principal component (PC1, thick gray line) estimated from the YECS SST anomalies. Note that we have plotted minus PC1 to show its out-of-phase relationship with the Siberian High especially for the period 1998–2014. The 11-year moving correlation coefficients (red line) between the PC1 and the Siberian High intensity and the moving averaged intensity of the Siberian High (green line) are illustrated in (b), with the first year of each moving period plotted on the x-axis.

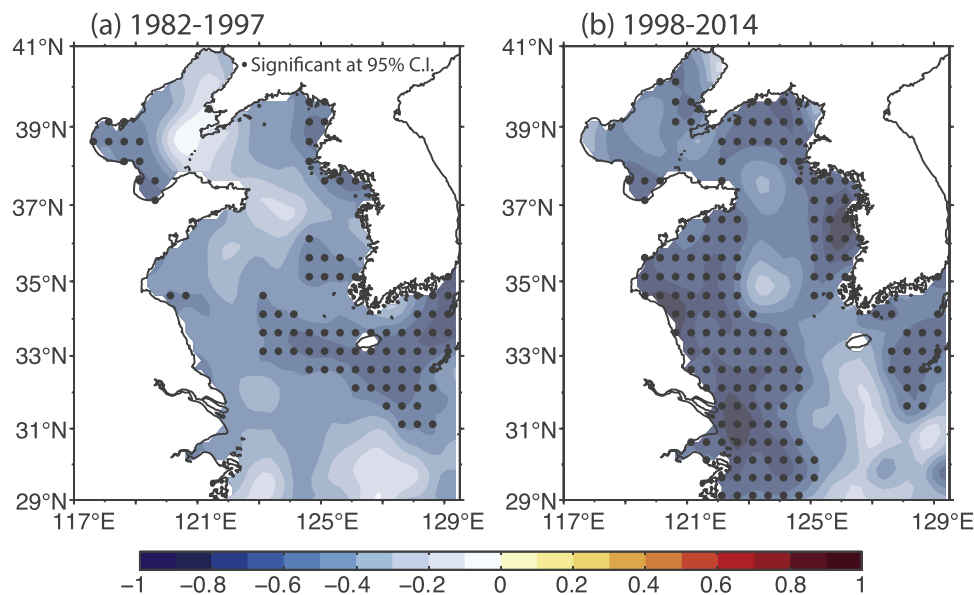


**Fig. 13.** Correlation maps between the time series of the standardized Siberian High intensity and the February–March–April mean SST anomalies for the periods (a) 1982–1997 and (b) 1998–2014. The dots superimposed on the correlation maps show the regions where the correlations are statistically significant at the 95% confidence level based on a student's *t*-test.

during the early years (1982–1997), while their out-of-phase relationship became significant with  $r = -0.62$  ( $p < 0.05$ ) during the recent years (1998–2014). In addition, a negative relationship between the SH index and the area-averaged winter net heat flux over the YECS also slightly increased ( $r = -0.77$ ) in the recent years. A moving correlation with an 11-year window (the red line in Fig. 12b) further demonstrates that its negative relationship between the PC1 and the SH index reached a significant level after 1997/1998 and then remained there. Another noteworthy feature is that the relationship between the index and the YECS SST tended to become more enhanced (see the red line in Fig. 12b) as the intensity of the SH became stronger (the green line in Fig. 12b): the correlation between these time series is  $-0.76$  ( $p < 0.05$ ). This increased connectivity between the SH pressure system and the YECS climate is further supported by a contrasting correlation pattern between the index and the FMA mean SST (Fig. 13): weak relationships throughout the broad region of the YECS during the earlier years vs. strong relationships during the recent years. Furthermore, this relationship is also in line with the wind-driven cooling demonstrated above, as well as anomalously cold winters in the Northern Hemisphere (Li and Wang, 2013; Liao et al., 2015).

Unsurprisingly, the region characterized by the relatively low relationships between the SST and the SH intensity at the center of the Yellow Sea coincides with the region showing weak cooling trends (Fig. 2c). These insignificant trends have been explained by a bathymetric effect, whereby relatively deep waters can act to attenuate the winter SST variation due to its larger heat capacity than the one for shallow waters (Xie et al., 2002; Park et al., 2015). The fact that the enhanced relationship between the SST and the KVT index is also observed in this region (see Fig. 8c) might reflect that the local oceanic advection is another contributor to both the insignificant trends and the observed weak SST responses to the SH along the central trough. Studies based on hydrographic observations and numerical experiments have suggested an in-phase relationship between the strength of the winter winds and the current speed of the upwind flow (e.g., Chen et al., 1994; Mask et al., 1998; Teague and Jacobs, 2000; Ichikawa and Beardsley, 2002; Ma et al., 2006; Moon et al., 2009; Lin et al., 2011; Lie and Cho, 2016; Tak et al., 2016). It can be inferred from these studies that the basin-scale surface cooling induced by the wind anomalies might be regionally compensated by the oceanic heat advection associated with the upwind flow. This theoretical approach basically agrees with Zhang et al. (2010), who demonstrated the damping role of the

oceanic advection on the PDO-related SST variance generated by the latent heat fluxes associated with winds.

## 7. Summary and concluding remarks

This study attempted to understand the low-frequency SST variability in the YECS and its relationship with large-scale atmospheric and oceanic processes for the period 1982–2014. The evolution of low-frequency SST is characterized by a decadal trend reversal from a robust warming trend until the late 1990s to a cooling one afterward. This variability is well demonstrated by the primary CSEOF mode, largely determined by the late winter SST. Further analysis suggests that wind anomalies in winter might contribute to the SST reversal at least in part: the strengthening (weakening) of the northwesterly winds leads to basin-scale sea surface cooling (warming) via the increased (decreased) losses of heat fluxes to the atmosphere during the recent (earlier) period after (before) the late 1990s.

The primary PC appeared to have a close correlation with the PDO index, but only before the regime shift in the North Pacific (i.e., 1982–1997). Further analyses indicate that the atmospheric/oceanic signals associated with the PDO were regionally confined to the eastern basin of the North Pacific after the regime shift, and concurrently resulted in the decoupling of the YECS climate from the PDO. The role of the PDO in determining the YECS SST seems to be superseded by the SH pressure system, which contributes to the intensified East Asian winter monsoon, thus resulting in basin-scale surface cooling over the YECS via the changes in the turbulent heat fluxes. Although the Kuroshio is not likely to contribute to a basin-scale change in the YECS SST, the upwind flow, an oceanic response to the northerly wind bursts during the winter monsoon, transports warm and saline waters along the central trough of the Yellow Sea, thereby locally counteracting the basin-scale cooling induced by the intensified SH pressure system during the recent period.

Our short analysis period makes it difficult to identify whether the recent cooling in the YECS could be attributed to internal natural variability (Liao et al., 2015) or can be regarded as a localized manifestation of anthropogenic warming (Li and Wang, 2013). A model-based comparison investigation between experiments for global warming and natural forcing scenarios might be required to explore the anthropogenic or natural contributions in shaping the YECS climate. In addition, a heat budget analysis based on a regional climate simulation

will help to assess the quantitative nature of diverse processes on the SST variability in the YECS.

## Acknowledgments

The authors thank the anonymous reviewers for their helpful comments. This work is a part of the projects entitled “Construction of Ocean Research Station and their Application Studies” and “Development of Korea Operational Oceanographic System (KOOS), Phase 2” funded by the Ministry of Oceans and Fisheries, Korea. SWY is supported by the Korea Meteorological Administration Research and Development Program under Grant KMIPA2015-1042.

## Appendix A. Supporting information

Supplementary data associated with this article can be found in the online version at <http://dx.doi.org/10.1016/j.csr.2018.01.009>.

## References

- Atlas, R., Hoffman, R.N., Ardizzone, J., Leidner, M., Jusem, J.C., 2009. Development of a new cross-calibrated, multi-platform (CCMP) ocean surface wind product. In: Proceedings of the 13th Conference on Integrated Observing and Assimilation Systems for Atmosphere, Oceans, and Land Surface (IOAS-AOLS), Phoenix, AZ, Amer. Meteor. Soc., 4B.1.
- Bao, B., Ren, G., 2014. Climatological characteristics and long-term change of SST over the marginal seas of China. *Cont. Shelf Res.* 77, 96–106. <http://dx.doi.org/10.1016/j.csr.2014.01.013>.
- Belkin, I.M., 2009. Rapid warming of large marine ecosystems. *Prog. Oceanogr.* 81, 207–213. <http://dx.doi.org/10.1016/j.pocean.2009.04.011>.
- Behringer, D.W., 2007. The global ocean data assimilation system (GODAS) at NCEP. In: Preprints, 11th Symp. on Integrated Observing and Assimilation Systems for the Atmosphere, Ocean, and Land Surface, San Antonio, TX, Amer. Meteor. Soc., 3.3.
- Bond, N.A., Overland, J.E., Spillane, M., Stabeno, P., 2003. Recent shifts in the state of the North Pacific. *Geophys. Res. Lett.* 30 (23), 2183. <http://dx.doi.org/10.1029/2003GL018597>.
- Bretherton, C.S., Widmann, M., Dymnikov, V.P., Wallace, J.M., Bladé, I., 1999. The effective number of spatial degrees of freedom of a time-varying field. *J. Clim.* 12, 1990–2009.
- Chen, C., Beardsley, R.C., Limeburner, R., Kim, K., 1994. Comparison of winter and summer hydrographic observations in the Yellow and East China Seas and adjacent Kuroshio during 1986. *Cont. Shelf Res.* 14 (7/8), 909–929.
- Chu, P.C., Wells, S.K., Haeger, S.D., Szczeczkowski, C., Carron, M., 1997. Temporal and spatial scales of the Yellow Sea thermal variability. *J. Geophys. Res.* 102 (C3), 5655–5667.
- Deser, C., Alexander, M.A., Xie, S.-P., Phillips, A.S., 2010. Sea surface temperature variability: patterns and mechanisms. *Annu. Rev. Mar. Sci.* 2, 115–143. <http://dx.doi.org/10.1146/annurev-marine-120408-151453>.
- Di Lorenzo, E., Schneider, N., Cobb, K.M., Franks, P.J.S., Chhak, K., Miller, A.J., McWilliams, J.C., Bograd, S.J., Arango, H., Curchitser, E., Powell, T.M., Rivière, P., 2008. North Pacific Gyre Oscillation links ocean climate and ecosystem change. *Geophys. Res. Lett.* 35, L08607. <http://dx.doi.org/10.1029/2007GL032838>.
- Di Lorenzo, E., Cobb, K.M., Furtado, J.C., Schneider, N., Anderson, B.T., Bracco, A., Alexander, M.A., Vimont, D.J., 2010. Central Pacific El Niño and decadal climate change in the North Pacific Ocean. *Nat. Geosci.* 3, 762–765. <http://dx.doi.org/10.1038/NGEO984>.
- Ding, R., Li, J., Tseng, Y.-H., Ruan, C., 2015. Influence of the North Pacific Victoria mode on the Pacific ITCZ summer precipitation. *J. Geophys. Res. Atmos.* 120, 964–979. <http://dx.doi.org/10.1002/2014JD022364>.
- Ding, Y., Liu, Y., Liang, S., Ma, X., Zhang, Y., Si, D., Liang, P., Song, Y., Zhang, J., 2014. Interdecadal variability of the East Asian winter monsoon and its possible links to global climate change. *J. Meteor. Res.* 28, 693–713.
- Hartmann, D.L., 2015. Pacific sea surface temperature and the winter of 2014. *Geophys. Res. Lett.* 42. <http://dx.doi.org/10.1002/2015GL063083>.
- Ichikawa, H., Beardsley, R.C., 2002. The current system in the Yellow and East China seas. *J. Oceanogr.* 58, 77–92. <http://dx.doi.org/10.1023/A:1015876701363>.
- Isobe, A., 2008. Recent advances in ocean circulation research on the Yellow Sea and East China Sea shelves. *J. Oceanogr.* 64 (4), 569–584.
- Jeong, J.-H., Ou, T., Linderholm, H.W., Kim, B.-M., Kim, S.-J., Kug, J.-S., Chen, D., 2011. Recent recovery of the Siberian High intensity. *J. Geophys. Res.* 116, D23102. <http://dx.doi.org/10.1029/2011JD015904>.
- Jo, H.-S., Yeh, S.-W., Lee, S.-K., 2015. Changes in the relationship in the SST variability between the tropical Pacific and the North Pacific across the 1998/1999 regime shift. *Geophys. Res. Lett.* 42, 7171–7178. <http://dx.doi.org/10.1002/2015GL065049>.
- Kim, K.-Y., 1997. Statistical interpolation using cyclostationary EOFs. *J. Clim.* 10, 2931–2942.
- Kim, K.-Y., Hamlington, B., Na, H., 2015. Theoretical foundation of cyclostationary EOF analysis for geophysical and climate variables: Concepts and examples. *Earth Sci. Rev.* 150, 201–218. <http://dx.doi.org/10.1016/j.earscirev.2015.06.003>.
- Kim, S.-J., Woo, S.-H., Kim, B.-M., Hur, S.-D., 2013. Trends in sea surface temperature change near the Korean Peninsula for the past 130 years. *Ocean Polar Res.* 33 (3), 281–290. <http://dx.doi.org/10.4217/OPR.2011.33.3.281>.
- Li, F., Wang, H., 2013. Spring surface cooling trend along the East Asian coast after the late 1990s. *Chin. Sci. Bull.* 58 (31), 3847–3851. <http://dx.doi.org/10.1007/s11434-013-5853-8>.
- Liao, E., Lu, W., Yan, X.-H., Jiang, Y., Kidwell, A., 2015. The coastal ocean response to the global warming acceleration and hiatus. *Sci. Rep.* 5, 16630. <http://dx.doi.org/10.1038/srep16630>.
- Lie, H.-J., Cho, C.-H., 2016. Seasonal circulation patterns of the Yellow and East China Seas derived from satellite-tracked drifter trajectories and hydrographic observations. *Prog. Oceanogr.* 146, 121–141. <http://dx.doi.org/10.1016/j.pocean.2016.06.004>.
- Lin, X., Yang, J., Guo, J., Zhang, Z., Yin, Y., Song, X., Zhang, X., 2011. An asymmetric upwind flow, Yellow Sea Warm Current: 1. New observations in the western Yellow Sea. *J. Geophys. Res. Ocean* 116 (C04026). <http://dx.doi.org/10.1029/2010JC006513>.
- Ma, J., Qiao, F., Xia, C., Kim, C.S., 2006. Effects of the Yellow Sea Warm Current on the winter temperature distribution in a numerical model. *J. Geophys. Res.* 111 (C11S04). <http://dx.doi.org/10.1029/2005JC003171>.
- Mantua, N.J., Hare, S.R., Zhang, Y., Wallace, J.M., Francis, R.C., 1997. A Pacific interdecadal climate oscillation with impacts on salmon production. *Bull. Am. Meteorol. Soc.* 78 (6), 1069–1079.
- Mask, A.C., O'Brien, J.J., Preller, R., 1998. Wind-driven effects on the Yellow Sea Warm Current. *J. Geophys. Res.* 103, 30713–30729. <http://dx.doi.org/10.1029/1998JC900007>.
- Moon, J.-H., Hirose, N., Yoon, J.-H., 2009. Comparison of wind and tidal contributions to seasonal circulation of the Yellow Sea. *J. Geophys. Res.* 114 (C08016). <http://dx.doi.org/10.1029/2009JC005314>.
- Na, J., Seo, J., Lie, H.J., 1999. Annual and seasonal variations of the sea surface heat fluxes in the East Asian marginal seas. *J. Oceanogr.* 55 (2), 257–270. <http://dx.doi.org/10.1023/A:100789160855>.
- Newman, M., Alexander, M.A., Ault, T.R., Cobb, K.M., Deser, C., Di Lorenzo, E., Mantua, N.J., Miller, A.J., Minobe, S., Nakamura, H., Schneider, N., Vimont, D.J., Phillips, A.S., Scott, J.D., Smith, C.A., 2016. The Pacific decadal oscillation, revisited. *J. Clim.* 29, 4399–4427. <http://dx.doi.org/10.1175/JCLI-D-15-0508.1>.
- Oey, L.-Y., Chang, M.-C., Chang, Y.-L., Lin, Y.-C., Xu, F.-H., 2013. Decadal warming of coastal China Seas and coupling with winter monsoon and currents. *Geophys. Res. Lett.* 40, 6288–6292. <http://dx.doi.org/10.1002/2013GL058202>.
- Overland, J., Rodionov, S., Minobe, S., Bond, N., 2008. North Pacific regime shifts: Definitions, issues and recent transitions. *Prog. Oceanogr.* 77, 92–102. <http://dx.doi.org/10.1016/j.pocean.2008.03.016>.
- Park, K.-A., Lee, E.-Y., Chang, E., Hong, S., 2015. Spatial and temporal variability of sea surface temperature and warming trends in the Yellow Sea. *J. Mar. Syst.* 143, 24–38. <http://dx.doi.org/10.1016/j.jmarsys.2014.10.013>.
- Park, T., Jang, C.J., Jungclaus, J.H., Haak, H., Park, W., Oh, I.-S., 2011. Effects of the Changjiang river discharge on sea surface warming in the Yellow and East China Seas in summer. *Cont. Shelf Res.* 31 (15–22), 1. <http://dx.doi.org/10.1016/j.csr.2010.10.012>.
- Park, W.-S., Oh, I.S., 2000. Interannual and interdecadal variations of sea surface temperature in the East Asian marginal seas. *Prog. Oceanogr.* 47, 191–204.
- Park, Y.-H., Yoon, J.-H., Youn, Y.-H., Vivier, F., 2012. Recent warming in the western North Pacific in relation to rapid changes in the atmospheric circulation of the Siberian High and Aleutian Low systems. *J. Clim.* 25, 3476–3493. <http://dx.doi.org/10.1175/2011JCLI4142.1>.
- Pei, Y.H., Liu, X.H., He, H.L., 2017. Interpreting the sea surface temperature warming trend in the Yellow Sea and East China Sea. *Sci. China Earth Sci.* 60 (10). <http://dx.doi.org/10.1007/s11430-017-9054-5>. (1588–1568).
- Peterson, W.T., Schwing, F.B., 2003. A new climate regime in Northeast Pacific ecosystems. *Geophys. Res. Lett.* 30 (17), 1896. <http://dx.doi.org/10.1029/2003GL017528>.
- Reynolds, R.W., Smith, T.M., Liu, C., Chelton, D.B., Casey, K.S., Schlax, M.G., 2007. Daily high-resolution-blended analyses for sea surface temperature. *J. Clim.* 20, 5473–5496. <http://dx.doi.org/10.1175/2007JCLI1824.1>.
- Reynolds, R.W., Chelton, D.B., 2010. Comparisons of daily sea surface temperature analyses for 2007–08. *J. Clim.* 23, 3545–3562.
- Stevenson, J.W., Niiler, P.P., 1983. Upper ocean heat budget during the Hawaii-to-Tahiti shuttle experiment. *J. Phys. Oceanogr.* 13, 1894–1907.
- Tak, Y.-J., Cho, Y.-K., Seo, G.-H., Choi, B.-J., 2016. Evolution of wind-driven flows in the Yellow Sea during winter. *J. Geophys. Res. Oceans* 121, 1970–1983. <http://dx.doi.org/10.1002/2016JC011622>.
- Teague, W.J., Jacobs, G.A., 2000. Current observations on the development of the Yellow Sea Warm Current. *J. Geophys. Res.* 105, 3401–3411. <http://dx.doi.org/10.1029/1999JC900301>.
- Trenberth, K.E., Jones, P.D., Ambenje, P., Bojariu, R., Easterling, D., Tank, A.K., Parker, D., Rahimzadeh, F., Renwick, J.A., Rusticucci, M., Soden, B., Zhai, P., 2007. Observations: surface and atmospheric climate change. In: Solomon, S., Qin, D., Manning, M., Chen, Z., Marquis, M., Averyt, K.B., Tignor, M., Miller, H.L. (Eds.), *Climate Change 2007: The Physical Science Basis. Contribution of Working Group I to the Fourth Assessment Report of the Intergovernmental Panel on Climate Change*. Cambridge University Press, Cambridge, United Kingdom, New York, NY, USA, pp. 235–236.
- Wang, B., Wu, R., Fu, X., 2000. Pacific–East Asian teleconnection: how does ENSO affect East Asian climate? *J. Clim.* 13, 1517–1536.
- Wang, F., Meng, Q., Tang, X., Hu, D., 2013. The long-term variability of sea surface temperature in the seas east of China in the past 40 a. *Acta Oceanol. Sin.* 32 (3), 48–53. <http://dx.doi.org/10.1007/s13131-013-0288-2>.
- Weare, B.C., 1989. Uncertainties in estimates of surface heat fluxes derived from marine reports over the tropical and subtropical oceans. *Tellus A* 41 (4), 35–37. <http://dx.doi.org/10.1034/j.1600-0834.1989.041001035.x>.

- [doi.org/10.3402/tellusa.v41i4.11846](http://doi.org/10.3402/tellusa.v41i4.11846).
- Wei, H., Yuan, C., Lu, Y., Zhang, Z., Luo, X., 2013. Forcing mechanisms of heat content variations in the Yellow Sea. *J. Geophys. Res. Ocean* 118, 4504–4513. <http://dx.doi.org/10.1002/jgrc.20326>.
- Wen, C., Kumar, A., Xue, Y., 2014. Factors contributing to uncertainty in Pacific Decadal Oscillation index. *Geophys. Res. Lett.* 41, 7980–7986. <http://dx.doi.org/10.1002/2014GL061992>.
- Wu, L., Liu, Z., 2003. Decadal variability in the North Pacific: the eastern North Pacific mode. *J. Clim.* 16, 3111–3131.
- Wu, R., Kirtman, B.P., Pégion, K., 2006. Local air-sea relationship in observations and model simulations. *J. Clim.* 19, 4914–4932.
- Wu, R., Lin, J., Li, B., 2016. Spatial and temporal variability of sea surface temperature in eastern marginal seas of China. *Adv. Meteorol.* <http://dx.doi.org/10.1155/2016/3820720>.
- Wu, R., Li, C., Lin, J., 2017. Enhanced winter warming in the Eastern China coastal waters and its relationship with ENSO. *Atmos. Sci. Lett.* 18, 11–18. <http://dx.doi.org/10.1002/asl.718>.
- Xiang, B., Wang, B., Li, T., 2013. A new paradigm for the predominance of standing Central Pacific Warming after the late 1990s. *Clim. Dyn.* 41 (2), 327–340. <http://dx.doi.org/10.1007/s00382-012-1427-8>.
- Xie, S.-P., Hafner, J., Tanimoto, Y., Liu, W.T., Tokinaga, H., Xu, H., 2002. Bathymetric effect on the winter sea surface temperature and climate of the Yellow and East China Seas. *Geophys. Res. Lett.* 29 (24), 2228. <http://dx.doi.org/10.1029/2002GL015884>.
- Xie, Y., Huang, J., Liu, Y., 2016. From accelerated warming to warming hiatus in China. *Int. J. Climatol.* 37 (4), 1758–1773. <http://dx.doi.org/10.1002/joc.4809>.
- Yan, X., Sun, C., 2015. An altimetric transport index for Kuroshio inflow northeast of Taiwan. *Sci. China Earth Sci.* 58 (5), 697–706. <http://dx.doi.org/10.1007/s11430-014-5024-z>.
- Yang, S.L., Xu, K.H., Milliman, J.D., Yang, H.F., Wu, C.S., 2015. Decline of Yangtze River water and sediment discharge: Impact from natural and anthropogenic changes. *Sci. Rep.* 5, 12581. <http://dx.doi.org/10.1038/srep12581>.
- Yeh, S.-W., Kug, J.-S., Dewitte, B., Kwon, M.-H., Kirtman, B.P., Jin, F.-F., 2009. El Niño in a changing climate. *Nature* 461, 511–514. <http://dx.doi.org/10.1038/nature08316>.
- Yeh, S.-W., Kim, C.-H., 2010. Recent warming in the Yellow/East China Sea during winter and the associated atmospheric circulation. *Cont. Shelf Res.* 30, 1428–1434. <http://dx.doi.org/10.1016/j.csr.2010.05.002>.
- Yeo, S.-R., Kim, K.-Y., Yeh, S.-W., Kim, W.-M., 2012. Decadal changes in the relationship between the tropical Pacific and the North Pacific. *J. Geophys. Res.* 117 (D15102). <http://dx.doi.org/10.1029/2012JD017775>.
- Yeo, S.-R., Kim, K.-Y., Yeh, S.-W., Kim, B.-M., Shim, T., Jhun, J.-G., 2014. Recent climate variation in the Bering and Chukchi seas and its linkages to large-scale circulation in the Pacific. *Clim. Dyn.* 42, 2423–2437. <http://dx.doi.org/10.1007/s00382-013-2042-z>.
- Yeo, S.-R., Kim, K.-Y., 2014. Global warming, low-frequency variability, and biennial oscillation: an attempt to understand the physical mechanisms driving major ENSO events. *Clim. Dyn.* 43, 771–786. <http://dx.doi.org/10.1007/s00382-013-1862-1>.
- Zhang, L., Wu, L., Lin, X., Wu, D., 2010. Modes and mechanisms of sea surface temperature low-frequency variations over the coastal China seas. *J. Geophys. Res.* 115 (C08031). <http://dx.doi.org/10.1029/2009JC006025>.